

UNIVERSITÀ DEGLI STUDI DI NAPOLI FEDERICO II



Department of Chemical Engineering, Materials and of the Industrial Production

Ph.D. in “Industrial Product and Process Engineering - XXX cycle”

“On the LFW T-Joints made via Electron Beam Melting and on
the study of the Ti6Al4V powder used in the EBM process”

Tutor:

Eng. Prof. Antonino Squillace

Ph.D. Candidate:

Liberini Mariacira

A.A. 2017-2018

Table of Contents

Abstract	1
1- Introduction.....	2
1.1 - The Additive Manufacturing Processes	2
1.2 – The Electron Beam Melting Process	7
1.3 - Linear Friction Welding.....	10
2.1- First Experimental Campaign: Traditional T-Joints.....	12
2.1.1- The Traditional T-Joints	12
2.2- Second Experimental campaign: The EMB T-Joints	17
2.3- Focus on The Ti6Al4V Powder used in the EBM Process	17
3- Results and Discussion	19
3.1 The Traditional T-Joints	19
3.1.1 Microstructural Analysis.....	19
3.1.2 Ultrasonic Controls	23
3.1.3 Final observation on Traditional T-Joints.....	27
3.2- The EBM T-Joints	29
3.2.1- Final observation on the EBM T-Joints.....	34
3.3- The Ti6Al4V Powder used in the EBM Process.....	34
4- Conclusions and Future Development.....	41
5- Bibliography.....	43

Abstract

The Additive Manufacturing (AM) is a group of processes that allow complex shape components to be realized from raw materials in the form of powders. The compaction of the powders is achieved by local melting of bed. Electron Beam Melting (EBM) is an additive manufacturing process in which a focalized electron beam is the heat source that allows the powders to be compacted. By EBM it is possible to realize complex shape components; this feature is of particular interest in titanium industry where numerous efforts are done to develop near net shape processes.

One of the limits of EBM based AM process is the difficulty to realize large dimension parts. This limit is due to the fact that the cabin, inside of which the process takes place, has maximum dimensions of 200x200x380 mm. Due to this limit the study of joining processes of different parts is of great interest. The Linear Friction Welding process has been choose because this welding technique leads to obtain joints with better mechanical properties with respect to the base material. The T-Joints have been chosen because this shape is useful both in aeronautical that in automotive field (i.e. bumpers) and because in literature a study on T-Joints obtained through LFW process has never been conducted.

In the present work the microstructure evolution of sheets of Ti6Al4V made by EBM and joined by Linear Friction Welding (LFW) is analyzed in details. In order to have the best performances from the LFW applied to the EBM ingots, a first experimental campaign on Traditional Ti6Al4V Joints has been conducted. The frequency and the forging force have been varied and the Traditional T-Joints have been studied in terms of ND Controls and Microstructure. The optimum LFW parameters in terms of frequency and forging force have been applied to the experimental campaign conducted on the EBM Joints. The experimental campaign conducted on the EBM Joints has been characterized by the SEM Observations. Different types of porosities have been observed inside both the base material and in the TMAZ and WZ. For this motivation, a focus on the Ti6Al4 powder used for the EBM process has been done and a full experimental campaign composed of SEM observations and statistical distribution analysis has been conducted.

1- Introduction

1.1 - The Additive Manufacturing Processes

The Additive Manufacturing Technologies is a wide range of different ways to make products layer upon layer in opposition with the technologies linked to the subtractive methods. In fact, ASTM has defined additive manufacturing (AM) as “a process of joining materials to make objects from 3D model data, usually layer upon layer, as opposed to subtractive manufacturing methodologies. Synonyms: additive fabrication, additive processes, additive techniques, additive layer manufacturing, layer manufacturing, and freeform fabrication” [1]. AM technologies can be applied to all classes of materials i.e.: metals, ceramics, polymers, composites, and biological systems. Until about two decades ago AM has been only a set of processes studied and improved in the Research field, now these group of technologies is more and more an important industrial manufacturing reality.

There is a study in literature that involves different aspects in AM [2]. The report explored important facets of the AM including:

- Design
- Process modeling and control
- Materials, processes, and machines
- Biomedical applications
- Energy and sustainability applications

Every field now it is a challenge to make these set of technologies useful in the modern industry to optimize the production and to get complicate products that with the standard technologies is not possible to realize.

Additive Manufacturing comes from the Rapid Prototyping and from the RP comes the basic principle of the technologies. The AM products are realized directly from the 3D-CAD model. The CAD model is divided in fixed thickness sublayers and the final object is generated through the subsequent solidification of the material involved layer per layer. In this way it is possible to get complicated geometries avoiding the problems linked to the difficulty of the machining. The object is realized adding material layer by layer. Each layer represents a thin transversal section

of the original CAD model. Obviously, every layer has a finite thickness, so the final product is an approximation of the original model and the thicker the layer the minor the approximation. In general, a typical layer is less than 150 μm .

For what regards metals, the main technologies use Laser or Electron Beam as heat source. The technologies that use the Laser (Selective Laser Melting, Selective Laser Sintering) has a different process of consolidation of the material depending on the source of the laser itself (CO₂ or Nd:YAG). This is due to the different wave length that can change the energy absorbed by the material. Depending on the laser source and on the laser parameters it can change the material, the modality of solidification of the layers, the mechanical properties of the final product and also the timing of production and the surface finishing. EBM technology manufactures parts by melting metal powder layer by layer with an electron beam in a high vacuum. In contrast to sintering techniques, both EBM and SLM achieve full melting of the metal powder.

All the technologies part of AM can be conducted to the same productive flow, each AM technology produces artifacts on a work plan and the vertical movements of the machine define the volume of work. Each machine has a kind of actuator unit, in most cases a laser beam/electron beam, which is responsible for building the particular layer by layer.

The common feature of all devices of AM is that "build tray" (fig.1), that is, the plane in which the piece is constructed. The build tray moves vertically only what is necessary during the production of a particular individual. Therefore, it is possible to divide the volume of work in two parts: the maximum working volume, defined by the size of the work plan and its maximum displacement, and the volume of the actual work, linked to the production of the specific product.

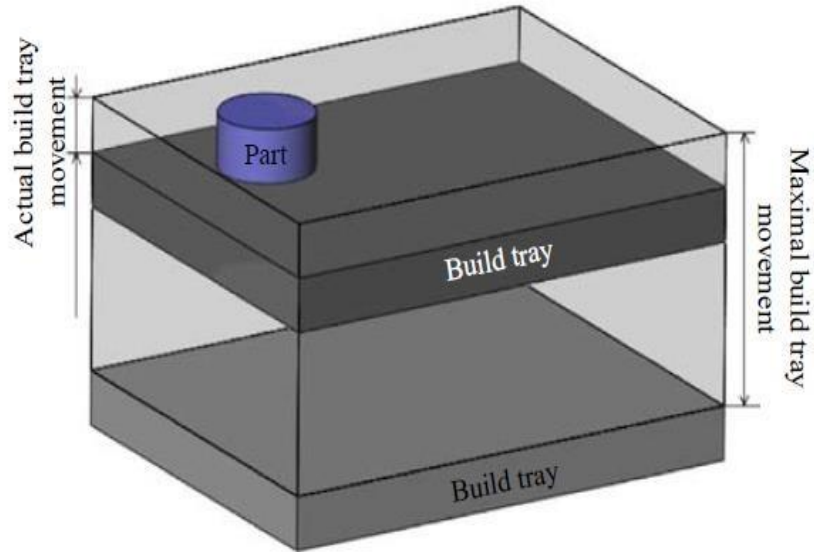


Fig. 1 – The Build Tray – The plane in which the part is built

The AM Technologies includes metallurgical, chemical and physical, non in equilibrium processes. These metallurgical processes show mechanisms of exchange of heat and mass and also chemical reactions. For these reasons the microstructural and mechanical characteristics of the products of AM Technologies could not be adequate to all the applications. According to the literature, the complex metallurgical phenomena depend on the powder use and from the process parameters. In particular, there is a strong dependence from: Chemical composition of the powder, dimension, shape and particles distribution of the powder and also, (for what regards the process), scanning velocity, dimension of the layers, power of the heat source. It is possible to achieve the coveted microstructure and mechanical characteristics of the final product by putting attention on powder and process parameters [1,3]. Although AM includes different technologies, all the possible alternatives can be conducted to one scheme of production that is composed by 8 steps, fig.2:



Fig. 2 – The 8 steps necessary to produce parts with AM Technologies

Step 1: CAD Model

The production of a part requires the elaboration of a detailed CAD model, which fully describes the external geometry

Step 2: STL Conversion

Almost all Additive Manufacturing plants are able to process STL files. In fact, STL files have become a standard. The STL format is an easy way to describe a CAD model only in terms of its geometry. This file is obtained from the CAD model by deleting all information except the outer surface of the model and approximating this surface with a series of triangular faces. The minimum dimension of such surfaces can be adjusted in almost all CAD modeling environments, with the aim of ensuring that the printed model does not show triangles on the surface. The approximation is estimated in terms of distance between the approximate triangular surface and the real surface that it should represent. There is the need to make this offset smaller

than the resolution of the print device. The conversion process of STL models is automated in almost all CAD systems, but errors may occur during this phase. There are a number of tools developed to better identify and correct such errors.

The STL files, in practice, contain information about the positions of the vertices of these triangles and normal surface vectors (to distinguish the interior from the outside). As a result, these files do not have information about the color or material of the model. This STL limit was recently exceeded by using the AMF format, which in fact includes also other useful information.

Step 3: Transfer and elaboration of STL file to the AM Plant

The STL file describing the part must be transferred to the Additive Manufacturing plant. Generally, there is the need to set the correct size, position, and orientation before processing the file for the production. It is common that multiple copies of the part to be realized are printed in a single process. This fact requires the original files to be scaled to be printed simultaneously. Some applications, however, require that printed parts have to be uniquely identified and for that purpose, some software have been developed to operate on the STL file to introduce simple features on the model, such as embossed characters.

Step 4: Setup of the AM plant

Before starting the actual print of a particular, there is the need to adjust process parameters. Some AM plants are designed to use specific materials and for this the user can adjust only few parameters, including the thickness of the layer. Other devices, on the other hand, are designed to fit a wide variety of materials, so they require the optimization of numerous parameters. In addition to process parameters, many machines require physical preparation before production. For example, the operator must check that there is enough raw material available in the AM plant. When the raw material is in the form of powder, it must also be sifted before being introduced into the molding plant.

Step 5: Printing

The realization of the product is an almost automatic process, in which the AM plant can operate without supervision. Only a superficial monitoring of the plant is needed to make sure that there are no errors, such as the interruption of the material flow or software problems.

Step 6: Rimotion of the part from the AM plant after printing

Once the plant has completed the implementation of the part, this must be removed. AM systems are equipped with safety devices that facilitate the safe removal of the parts, ensuring, for example, that working temperatures are sufficiently low or that there are no moving parts inside the plant.

Step 7: Post-Processing

After the printing, the products can require some thermal treatments or also the products can have some support systems that have to be removed.

Step 8: Application

At this point the components are ready to be used. However, sometimes further treatments are needed before the parts can actually be used, for example to obtain the right surface finish. On the other hand, the raw materials in form of powder used in some AM processes have limited duration and must be stored under controlled conditions to prevent undesirable chemical reactions. If repeated several times, the recovery may degrade material properties [3].

1.2 – The Electron Beam Melting Process

Electron beam melting (EBM) is a metal powder bed fusion additive manufacturing (AM) technology used for the fabrication of three dimensional near-net-shaped functional components directly from CAD models [4].

Electron Beam Melting technology leads to produce prototypes, or a series of products, directly in metal, ready to be tested or used as final components. The technology lends itself perfectly to the re-engineering. EBM Technology is almost indicated for the realization of the products in the biomedical and orthopedic fields and also in the aeronautic field.

The Electron Beam Melting technology allows the metal to be merged thanks to a concentrated electron beam, accelerated and directed against the metal powder layer. The process, starting directly from the material in the form of micro powder (granulometry 45-80 μm), allows to produce final and density components close to 100%. EBM technology is quite similar to SLM (or DMLS), where the dust is deposited in very thin layers (50 micrometers) in a vacuum

chamber (hence without oxygen) with a constant pre-heating of the dust cover (for example titanium Ti64 is about 740°C), with high melting capacity (up to 80 cm³/h).

The electronic beam can concentrate a melting power greater than the one of the laser beam, due to the considerable atomic mass difference between the electron and the photon. The Electron Beam Melting system can easily achieve melting temperatures between 700 and 1400°C (or even further). Thanks to this reason, a wide range of materials that are of difficult processing for what concerns the traditional technologies for casting and chip removal, such as titanium alumina (□Ti-Al) or titanium alloys with Niobium or other elements, can be easily used. The EBM process is a "hot" process, where powders are maintained at a high and constant temperature throughout all the fusion process, unlike the laser processes called "cold", because the metal micropowders are fused at a temperature close to the ambient temperature or never above 200°C. The EBM Technology leads the products substantially free from residual stresses and therefore the parts do not require thermal fusion after fusion treatments.

The application of AM technologies in general, and of EBM in particular, is undergoing a great increase both in variety and in quantity of different applications. Due to the progresses made in the field of AM technologies and also in EBM technology, a wider range of industries are studying and implementing these technologies to produce an increasingly diverse range of products. Biomedical implant applications and structural aerospace parts are the most promising areas for EBM technology. However, the development of EBM technology in these areas is slowed down by the lack of fundamental knowledge, consistent databases, and standardization which are all critical in these industry sectors [5-7]. The energy source for the melting process is an electron beam emitted from a tungsten filament. This beam is controlled by two magnetic coils. The coils can focus, control, and vary the position and the diameter of the beam. The manufacturing parameters are generated and controlled by a software in order to fabricate the products with improved mechanical properties, low porosity and surface roughness, and optimized geometrical reproducibility. This software creates scanning algorithms based on the geometry of the part to be manufactured. The main parameters controlled by the software are: minimum and maximum beam current, number of times the beam scan is to be repeated, scanning speed of the electron beam, distance between individual scan lines (line offset), line order for the hatch pattern, and rotation angle between consecutive hatches [8]. This work is focused on the Ti-6Al-6V products.

Microstructure evolution and mechanical properties have been studied for Ti-6Al-4V alloys due to its versatility resulting from the good balance between mechanical properties, castability, plastic workability, heat treatability, and weldability [9]. Ti-6Al-4V has been applied in industry and studied in the laboratory, resulting in an extensive knowledgebase relative to other metal alloys fabricated by this technology. Heat treatment of AM Ti-6Al-4V for different technologies has been extensively studied with the purpose of relieving stress and achieving an equilibrium microstructure, eliminating the metastable α' martensite phase and obtaining a microstructure with exclusively α and β phases [10]. However for the EBM technology, the relation between microstructure and mechanical properties has been mainly limited to the as-fabricated condition, except for some cases where hot isostatic pressing (HIP) was applied to the EBM parts. The EBM process, similarly to other AM processes, does not completely prevent the presence of porosity in the build. Therefore, in order to mitigate the disadvantages caused by these defects, the effect of HIP treatment has been studied [11–13]. The biggest interest for the study of the mechanical properties in the as-fabricated condition is that the EBM process, unlike other metal AM technologies such as selective laser melting (SLM) or laser engineered net shaping (LENS), does not require heat treatment to obtain reasonable ductility and low residual stresses. The high temperature of the fabrication chamber in the EBM process prevents the presence of brittle α' martensitic phase from forming in the final microstructure, while the slow cooling rates from the chamber temperature to room temperature, relieves most of the residual stress generated during the additive manufacturing process [11].

Ti-6Al-4V is an $\alpha+\beta$ alloy because α and β microstructural phases coexist at room temperature. The $\alpha+\beta$ alloys are interesting because they combine the strength of α alloys with the ductility of β alloys, and their microstructures and properties can be varied widely by appropriate heat treatments and thermomechanical processing [14-17]. The current study focuses on understanding the effect of different heat treatments on the unique microstructure of the EBM Ti6Al-4V ELI (Extra Low Interstitial) and its impact on mechanical properties.

Other information on AM Technologies and on EBM can be find in literature [18].

1.3 - Linear Friction Welding

Linear friction welding is a solid state welding technique. It uses the heat generated by the relative motion of the two parts to be jointed and the compression force to create a junction. Friction and thermal stress are the main developers of the softening and continuous plasticization of the interface zone between the two parts to be soldered. The junction interface is characterized by a central welding zone (weld zone) and, near the latter, there is the Thermal Mechanically Affected Zone (TMAZ). [19] LFW can be characterized in four phases: the initial phase, the transition phase, the balance phase, and the deceleration phase:

- Initial phase: the two components are placed in contact between them with a light pressure and one of them moves with alternate straight motion, generating heat. To achieve an adequate level of plasticization at the interface, the alternative motion must generate enough heat to overcome the conduction losses (occurring in the base metal areas away from the contact area) and radiation and convection losses (occurring towards the environment).
- Transition phase: Part of the material is ejected from the interface as "flash" (very thin metal sheets) while the softened layer between the two parts undergoes a plastic deformation due to the high axial load. At this stage, the TMAZ begins to spread to the base material, starting from the contact area.
- Balance phase: A significant axial shortening is obtained, since part of the material has been expelled in the previous step. The TMAZ continues to progress during the equilibrium phase as the heat is transmitted far from the interface zone.
- Deceleration phase: A rapid stop of relative motion is imposed and the application of a forging pressure is given to consolidate the welding.

As already mentioned, the junction interface is characterized by two zones: the weld zone and the TMAZ. In the titanium alloy Ti-6Al-4V, the microstructure of the weld zone is typically composed by very thin lamellas (<10 μ m) confined within the edges of the β grains. This indicates that the structure (deformed) was dynamically recrystallized during LFW, following a brief exposure to temperatures higher than the β -transus Temperature. Experimental tests have

established that this welding portion is characterized by higher mechanical properties in terms of hardness reaching values of about 370-400 HV (clearly related to the fine grain microstructure). The frequency and the amplitude are the two process parameters that have the greatest impact on the weld quality, in terms of hardness, width of the weld regions and width of the TMAZ, and also on the shortening phenomena occurring during the Balance Phase of the process. [20] The LFW offers a number of advantages with respect to the traditional welding processes:

- Quality: The quality and the resistance of the junction are remarkable despite the traditional welding processes
- Type of material: LFW is the ideal technique for materials that are difficult to be welded with conventional methods due to the fact that there is no need to achieve the fusion temperature of the material itself. It also makes possible the junction of two parts constituted by two different metallic alloys and this is very important in the aeronautic field in which there is the necessity to joint parts with different mechanical and chemical characteristics ;
- Welding Zone: Good mechanical properties and low overall distortion of welding zone are detected;
- Energy saving: No external heat sources are needed and also relative speeds are low;
- Safety: Total absence of volatile toxic substances, fumes or sprays of molten material;
- Automation: The simplicity of the process makes it possible to have ample automation possibilities;
- No need of specific tools, the plant of LFW can be customized on the base of the parts to be welded. The only tool is composed by two pliers that hang the parts and by the alimentation of the plant itself.

Other information on the LFW can be founded in literature [21-24].

2- Materials and Methods

This work is developed in two parts. During the first part of the work, the experimental tests put the focus on T-Joints in Ti-6Al-4V obtained from ingots get by traditional casting technology. The T-Shape wants put the attention on the fact that until now the LFW technique has been applied only on butt joints, but in industry there is the need to weld parts with different geometry and often without symmetry. Through this first experimental campaign an optimization of the process parameters has been performed and also through the NDI controls a map of the joints has been find out. During the second part of the work, the experimental campaign has been conducted on T-Joint obtained from ingots produced with the EBM technology, in order to observe the final microstructure and to study the mechanical properties of the EMB Joints. The LFW plants has been studied and developed based on literature studies [23, 24] due to the fact that these kind of plant can be built and customized according the shape and dimensions of the parts to be welded.

2.1- First Experimental Campaign: Traditional T-Joints

Aiming to prove the effectiveness of the ultrasonic control in detecting the welding defects, different joints in different processing conditions were manufactured to simulate the diverse defects and metallurgies that could be obtained through the LFW process. The ultrasonic control was effectuated on all the joints. After that a full experimental campaign, including microstructural observation, was carried out on the joints to confirm the results of the ultrasonic control. In the hereinafter the whole experimentation will be presented and discussed in details.

2.1.1- The Traditional T-Joints

In this research activity Ti6Al4V ingots were used as base material, both the mechanical properties and the chemical composition were fully available in literature and were not here reported for the sake of brevity [25]. The specimens to be welded were machined from the ingots, parallelepiped blocks in two different dimensions were produced: blocks “A” 64 mm x 26 mm x 8.6 mm and blocks “B” 40 mm x 26 mm x 11 mm (the welding configuration is

sketched in Fig. 3.a. Such a decision, to weld together pieces of different dimensions, to simulate some real aeronautical applications (e.g., bumpers or blisks). The alternate linear movement was imposed to the block “A” while the force was applied to the block “B”. The movement was imposed from left to right. After the machining no further preparation of the blocks before the welding is required. The contact area between the two pieces during the welding is 26 mm x 11 mm. The welding process was effectuated by means of an in-house developed LFW-fixture, as shown in Fig.3.

The welding equipment consists of four main components: the hydraulic unit, a battery of accumulators, the electrical panel and the LFW fixture. The fixture is composed by a support structure on which two hydraulic pistons are placed, arranged orthogonally between them and to which are connected the actuators and the clamps that grip the two parts to be welded. The transverse actuator can execute a rectilinear motion with a maximum frequency value of 70 Hz and it can also apply a maximum compression load of 70000 N, the other actuator can exert a maximum value of the forging load of 100000 N. The hydraulic unit is constituted by a gear pump fed and by a 18 kW asynchronous motor. The motor has to feed the battery of accumulators with the engine oil at a pressure of 20MPa. The battery of six accumulators, with a total capacity of 120L, has the aim to ensure the supply of oil to the transverse actuator during welding process.

In order to obtain joints with different characteristics (i.e., joints free from defects, joints with defects of different dimensions and positions, joints with different metallurgies) the main process parameters were varied in a wide range. Tab. 1 shows the process parameters adopted for all the different joints manufactured. An oscillation amplitude of 15 mm was adopted in all the tests. For each sample three different joints were manufactured and tested to ensure the repeatability of the process.

The process parameters were chosen on the basis of trials experiments (not reported here) for the sake of brevity and taking into account the previously mentioned literature. In literature [26] can be found the study of the LFW process for the Ti6Al4V and discussed the effect of the process parameters on the metallurgy of the joints, and a detailed review on the LFW process where a lot of information concerning the process parameters also could be found in [27]. Moreover, it can be seen from Tab.1 that only two distinct values for the forging force are adopted because this

parameter has less influence on the final characteristics of the joints with respect to the other process parameters [28].

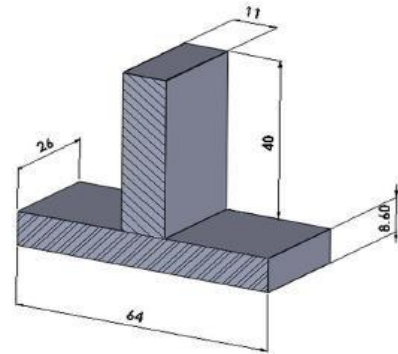


Fig. 3: 3.a – The LFW Plant used for the experimental campaign on the Traditional T-Joints and also on the EBM T-Joints; 3.b- Final Dimensions of the ingots (both for the traditional T-Joints and for the EBM T-Joints) forming the joints

Sample No.	Oscillation frequency f /Hz	Oscillation time t /ms	Friction force N	Friction pressure /MPa	Forging force N	Forging pressure /MPa	Axial shortening /mm
1	30	5 000	5 500	19.23	6 000	20.98	5
2	40	3 500	5 500	19.23	8 700	30.42	6
3	45	3 500	5 500	19.23	8 700	30.42	6
4	45	5 000	7 250	25.35	11 600	40.56	6
5	36	5 000	5 500	19.23	8 700	30.42	6
6	36	3 500	7 250	25.35	11 600	40.56	6

Tab. 1 – Process Parameters used for the manufacturing of the Traditional T-Joints.

2.1.2- Ultrasonic Control

The joints were inspected by means of a US Multi2000 Pocket 16-9-64 equipment. The inspection was carried out by using a single probe, DS 6 HB 2-7 produced by KARL DEUTSCH, 5MHz. The main technical features of the probe are given in Tab.2. This low frequency probe ($f = 5$ MHz) was chosen in order to obtain an important decrease of the signal attenuation and a more efficient measure [29]. The operational mode chosen was the reflection: the probe was used for the emission and the reception of ultrasonic waves. During the acquisition the pulse echo technique was adopted: short-duration ultrasound pulses were transmitted into the region to be studied, and the echo signals resulting from scattering and reflection were acquired and displayed. The depth of a reflective structure is inferred from the

delay between pulse transmission and echo reception [30]. The data presentation method was a scan by which intelligence signals from a signal object located were displayed. As generally applied to pulse echo ultrasonic, the horizontal sweep is proportional to distance and the vertical one is proportional to amplitude. Thus the location and magnitude of acoustical interface are indicated as to depth below the transducer. The specimens were tested before and after the welding in order to evaluate the sample integrity and calibrate the acquisition system. By properly setting the gate, a fairly clear picture of the welded area is obtained, and then it is preceded successively to a correct sizing of the defect. Echo Max (abs) is the used detection mode: once the gate is set on the implementation of the scan, it will be registered only the maximum peak that surpasses it. So, using a non-welded component, the correct thickness is obtained (see Fig. 4) and the acquisition system is calibrated. The propagation velocity, equal to 5000mm/s, is registered. The sensitivity of the control, i.e., the minimum detectable defect size d^* , strictly depends on the wavelength of the ultrasound beam, λ . A defect is detectable only when its transverse dimension, with respect to the propagation direction, is at least equal to $\lambda/4$. Smaller defects cannot be observed. Due to the material and probe characteristics, the control can display defects (discontinuity or inclusions) whose transverse dimension is bigger than two tenths of a millimeter ($\lambda/4 = 0.25$ mm). In order to scan the welded zone, the T-joint specimens were cut to intercept cracks on the cut surface. Fig.5 indicates the points where the ultrasound probe is positioned.

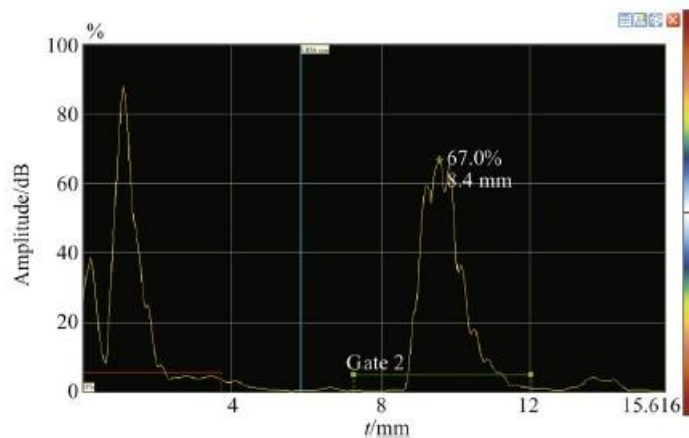


Fig. 4 - Output of the ultrasonic control carried out on an “A” block used to calibrate the measurement system

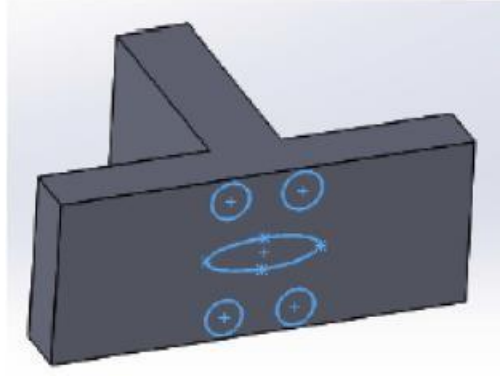


Fig. 5 - Points where the ultrasonic control was carried out, i.e., points where the probe was placed during the control

2.1.3- Microstructural Observation

The specimens for the metallographic observations were cut from the cross section of the joints by following the cutting scheme, as shown in Fig.6. The specimens were cut by means of a metallographic precision cutting machine, mounted in a thermoset conductive resin, and then polished to a mirror like surface finishing. The specimens were etched using a hydrofluoridric acid solution. All the above mentioned procedures were carried out following the ASTM standards for metallography. Finally the prepared specimens were observed through a Hitachi TM3000 SEM.

Moreover the dimension of the grains and the extension of the different metallurgical zones were measured through the image analysis software as done in previous works [31].

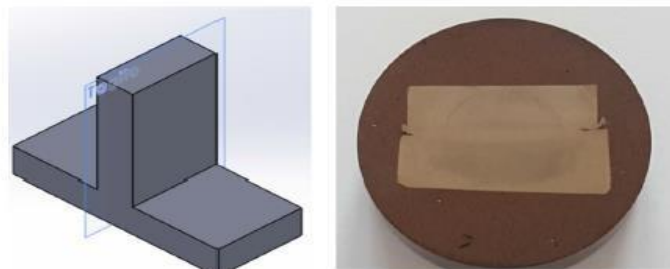


Fig. 6 - Cutting scheme of the joints to obtain the metallographic specimens

2.2- Second Experimental campaign: The EMB T-Joints

Based on the literature and on the previous studied (first experimental campaign), the second experimental campaign has been conducted on 10 samples with fixed LFW process parameters. EBM specimen suitable for LFW were prepared by CIRA (Centro Italiano Ricerche Aerospaziali) using an ARCAM A2X facility. The specimen is reported in Fig. 7. The specimens were joined using the machine described before, the parameters used in the welding process have been find out thanks to the first experimental campaign on Traditional T-Joints, as it will be discussed later. The dimensions of the EBM ingots are the same described before.



Fig. 7- EBM Specimen Before and After the welding process

2.3- Focus on The Ti6Al4V Powder used in the EBM Process

Gas atomized Ti-6Al-4V powders, showing a regular spherical shape, were used for the EBM processes. The size of the particles was measured via image analysis software. Both mechanical and chemical properties of this alloy are fully available in the literature [32].

Gas atomization is an industrial process in which a liquid flux of a molten alloy is disintegrated by an high velocity gas, solidifying the metal into powder micro-particles, without any contact with the container and with a cooling rate in the order of 10^3 - 10^4 °C/s, depending on the particle size. The molten material forms an axial flowing stream with the aid of an argon flux injected under sufficient pressure through an injection nozzle. Around and along the axially flowing molten an annular stream of atomizing gas is formed. The atomizing gas is generally an inert or

substantially inert gas such as argon, helium or nitrogen. The atomizing gas is injected under pressure, generally within the range of 5-170 bar, at an angle, causing the annular gas stream to swirl circumferentially around the molten stream, and to diverge in an outwardly forming cone from the injection point.

Concerning the EBM process, an ARCAM A2X (full specifications are available online) machine was used, and the process parameters were the optimal ones suggested by ARCAM on the basis of their experience. The building process was carried out under vacuum conditions. The building process was carried out in a chamber ventilated with a controlled argon flux.

The microstructure of the manufactured components was studied through metallographic observations. The metallographic specimens were cut from the additive manufactured components through a precision hacksaw, as prescribed by the ASTM E3-11 standard. After that the specimens were mounted in a thermoset resin and polished to a mirror-like finishing. After the polishing, the specimens were rinsed with ethanol in an ultrasonic bath, followed by chemical etching using hydrofluoric acid. The microstructure of the powder, as supplied, was also investigated. This was done in order to study the genesis of the defects that can be observed in the final component. The procedure adopted to observe the microstructure of the particles is hereinafter reported. Powder specks were mixed with an epoxy glue on a little metal plate. After 12 h, the prepared specimen was hot mounted into an hardener hot conductive resin by using an automatic mounting machine. Afterward, the specimen was prepared by following the sequent route. Firstly, the external surface was grinded with a P80 sandpaper until when the mixture of glue and powders was visible on the specimen surface. In a second step, P320, P600 and P1000 sandpapers were used (1 min 30 s. 20 N each). The polishing was performed with diamond paste with granulometry between 9 and 1 μm . The specimen preparation was completed with an ultrasonic bath (15 min.) in ethanol. After that, the specimen was chemically etched following the same procedure as for the specimens cut from the printed parts. The preparation route can be summarized in the following steps: powder specks mix, hot mounting into an hardener hot conductive resin, specimen grinding, ultrasonic bath in ethanol, chemical etching.

3- Results and Discussion

In this paragraph the results regarding the full experimental campaign conducted will be reported and discussed, starting from the Traditional T-Joints and ending with the focus performed on the Ti6Al4V powder.

3.1 The Traditional T-Joints

3.1.1 Microstructural Analysis

Figure 8 shows a micrograph representing the microstructure of the base material. A bimodal microstructure can be observed, made of coarse α grains immersed in an $\alpha+\beta$ matrix. This kind of microstructure is typical of annealed Ti6Al4V ingots.

Concerning the final microstructure of the joints three main different metallurgical zones can be highlighted from the center of the joint including the welding region, the TMAZ and the base material. Regarding the base material in this region the material retains the parent microstructure, i.e., retains the microstructure, as shown in Fig. 8. In figure 9 is reported a micrograph of the microstructure observed in the TMAZ.

The microstructure of the TMAZ is made of α grains within an $\alpha+\beta$ matrix. The α grains are stretched along a direction that is quite perpendicular to the plunging direction of the welding process. The grains are deformed and are highly oriented. Moreover it is possible to assess that the longitudinal dimension of the α grains, which is an index of the crushing suffered from the same grains, depends on the number of cycles impressed to the samples. In this zone the grains are not fully recrystallized. Figure 10 shows a fully recrystallized microstructure regarding the welded zone (WZ). It is possible to observe a fully lamellar microstructure, Widmanstatten like, contained in the former β grain boundaries.

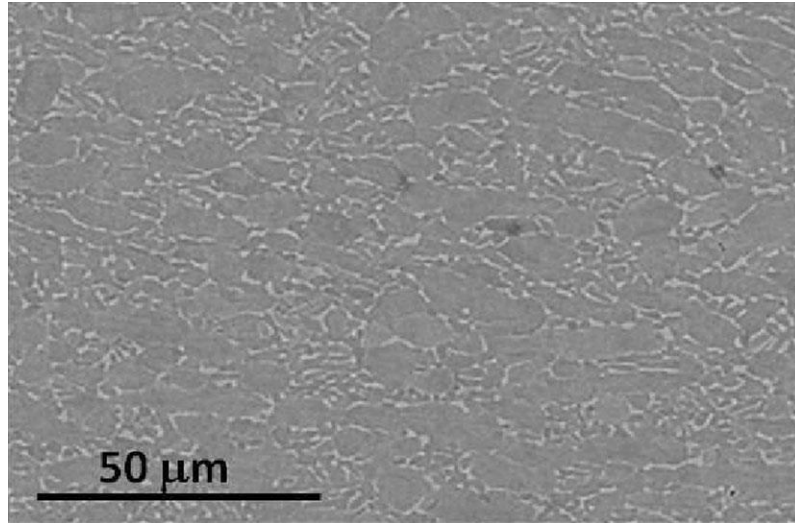


Fig. 8 – Micrograph of the base material of the joints

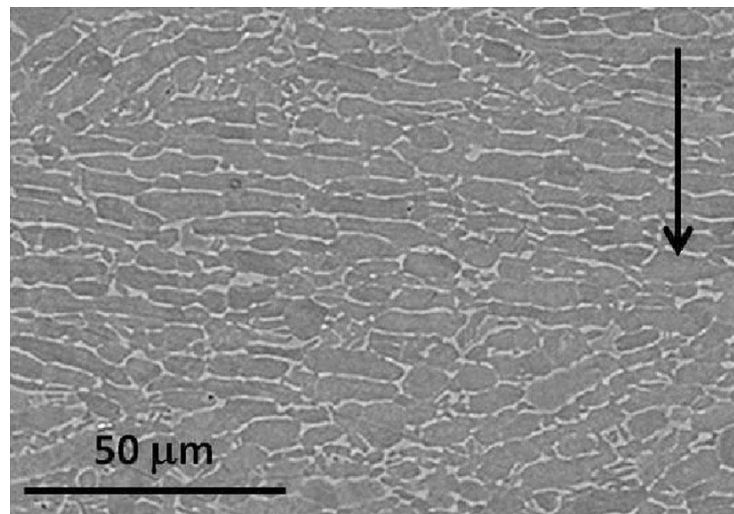


Fig. 9 – Cross section micrograph of the TMAZ (the arrow highlights the plunging direction during the welding)

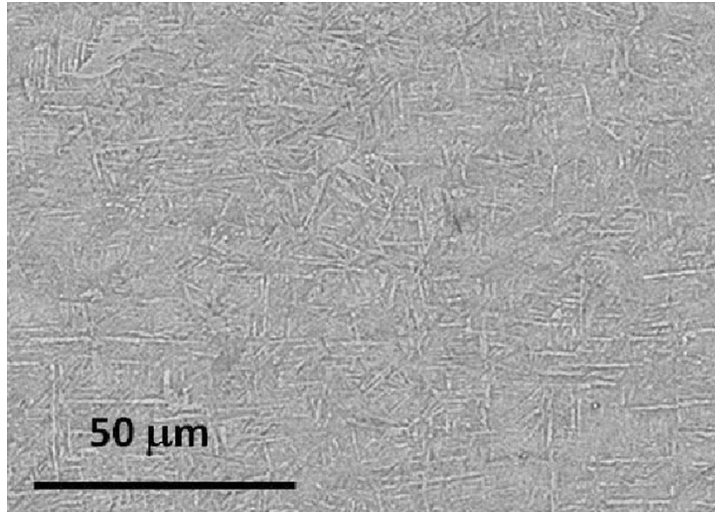


Fig. 10 – Micrography of the WZ totally re-crystallized

Moreover some martensitic grains are also appreciable. This microstructure is produced due to the fast cooling from the β region experienced by the material. The material in the welding region reached a temperature higher than the β transus one due to the high amount of frictional heat produced during the welding, so the microstructure experienced a fully recrystallization resulting in the complete β transformation. After the welding process, the material experiences a fast cooling resulting in the observed multi-oriented lamellar microstructure. The above described microstructural evolution is coherent with what discussed in the introduction section. Moreover this microstructural evolution is, from a qualitative point of view, the same for all the different joints under investigation.

The differences that can be observed among the joints manufactured with different sets of the process parameters are grain dimensions, extension of the different metallurgical zones, and presence of defects. In particular the dimensions of the α strips depend on the process parameters used. In order to better discuss the results a new parameter is introduced to group the frequency of oscillation and the oscillation time. The number of cycles that is the number of oscillation experienced by the pieces to be welded and is defined as the product between the frequency and the time. Figure 11.a shows the grain size in both the TMAZ and the WZ as a function of the number of cycles. Figure 11.b shows the grain size in both the TMAZ and the WZ as a function of the forging force.

It is possible to observe that the size of the lamellae increases with the increasing of the number of cycles and also with the decreasing of the forging force applied. As above described the formation of lamellae is due to the physical phenomena and the phase transition that occur during the slow cooling from the β region. The final dimensions of the lamellae can be addressed to the recrystallization phenomena that take place during the welding due to the severe plastic deformation experienced by the components joined. As reported in literature [33], when a metal experiences a severe plastic deformation at high temperatures, two different recrystallization phases are observed, i.e., primary and secondary recrystallization.

This is the case of the LFW process. The primary recrystallization is ruled by several laws described in literature [33, 34], in particular it is demonstrated that the final grain size depends chiefly upon the degree of deformation and to a lesser degree upon the temperature, normally being smaller the greater the degree of deformation and the lower the temperature. Moreover for a given degree of deformation a higher working temperature entails a coarser recrystallized grain size. These rules can be used to explain the results, as shown in Fig. 11. It is possible to observe that the dimension of the lamellae decreases with the increasing of the forging force. At this stage it is important to highlight that an increasing of the forging force leads to an increasing of the degree of deformation, so the data in Fig. 11 suggests that the lamellae becomes coarser with the decreasing of the degree of deformation, such a result is in agree with the above mentioned laws. It is also possible to note that the size of the lamellae increases with the increases with the increasing of the number of cycles. The increase of the number of cycles leads to an increasing of the frictional heat produced that involves the reaching of higher temperatures during the welding. Once again the observed results can be explained on the basis of the recrystallization laws, i.e., the lamellae becomes coarser with the increasing of the processing temperature.

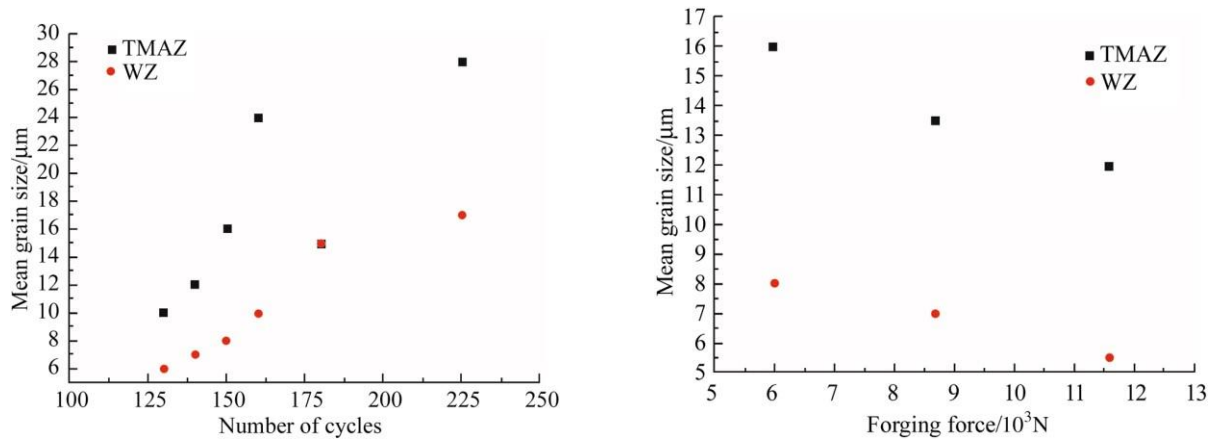


Fig. 11 - Mean dimension of the lamellae in both the TMAZ and the WZ against the number of cycle and the forging force

3.1.2 Ultrasonic Controls

The fig. 12 show the sample processed at 30Hz. This sample is the only one that presents a defect in the middle of the welding at 7 mm of depth. This defect can be observed with a macrograph picture, so according to this first analysis we can resume that the frequency of 30Hz is not sufficient to generate the quantity of heat flow to get an homogeneous welding and TMAZ zone. To show how the ultrasonic signal detect the defect, in fig. 14 will be reported the micrographic picture of the defect and the co-respective ultrasonic detection. Fig. 13 shows the outputs of the ultrasonic control for three different joints, and all of them are free from defects. In particular, the joints respectively processed at 36, 40 and 45 Hz have been reported.

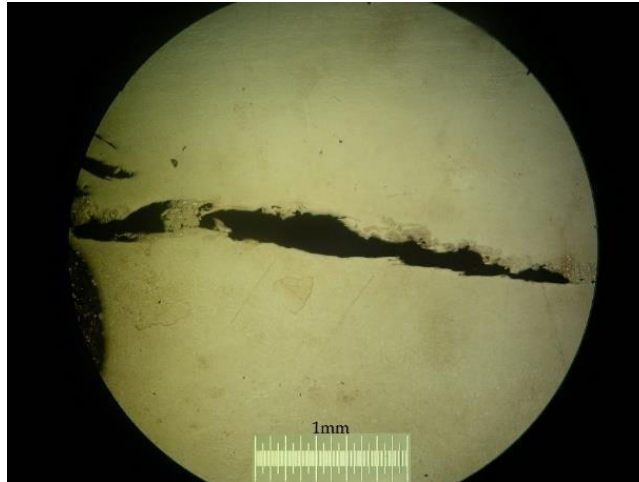


Fig. 12 - Sample processed at 30Hz. As it is possible to observe there is a solution of continuity inside the welding.

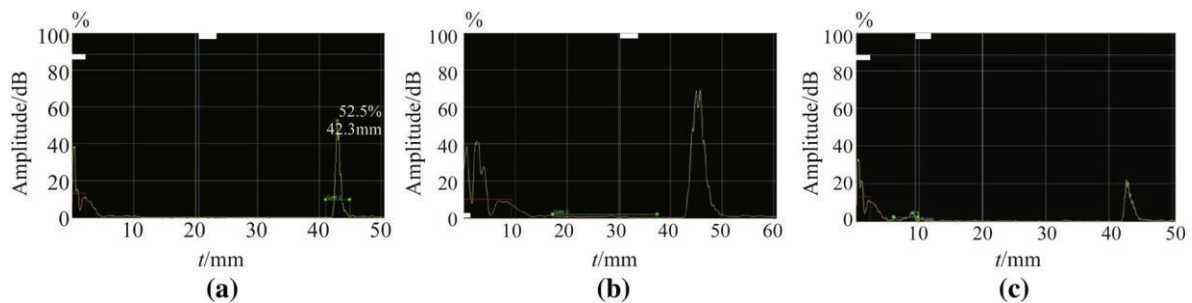


Fig. 13 - Result of the ultrasonic control in the welding zone of three different joints free from defects

It is possible to observe, for all the joints, that only the input and the bottom echoes are visible. This is due to the fact that the joints are totally free from defects in the welding and TMAZ zone. Moreover it is possible to observe that the output echoes of the different joints have different amplitude, which suggest that the extension of the different metallurgical zones influences the ultrasonic signal.

Figure 14 shows a defect that can be found in an LFW joint (when the processing conditions are not properly set, i.e. sample processed at 30Hz), an internal porosity, and the respective output of the ultrasonic control. It is possible to observe a peak between the input and the bottom echoes, and this peak is due to the aforementioned defect. The position and the intensity of this peak suggest the position and the dimension of the detected defect. Figure 15 shows the

macrograph of a joint processed at 36 Hz with lowest Forging Force charge (5500N) with a big internal defect and the respective output of the ultrasonic control. In this case it is possible to observe, looking at the output of the ultrasonic control, the input peak and the one related to the defect. Conversely the output peak is not visible, and this can be explained that the huge internal defect induces a big damping down of the signal.

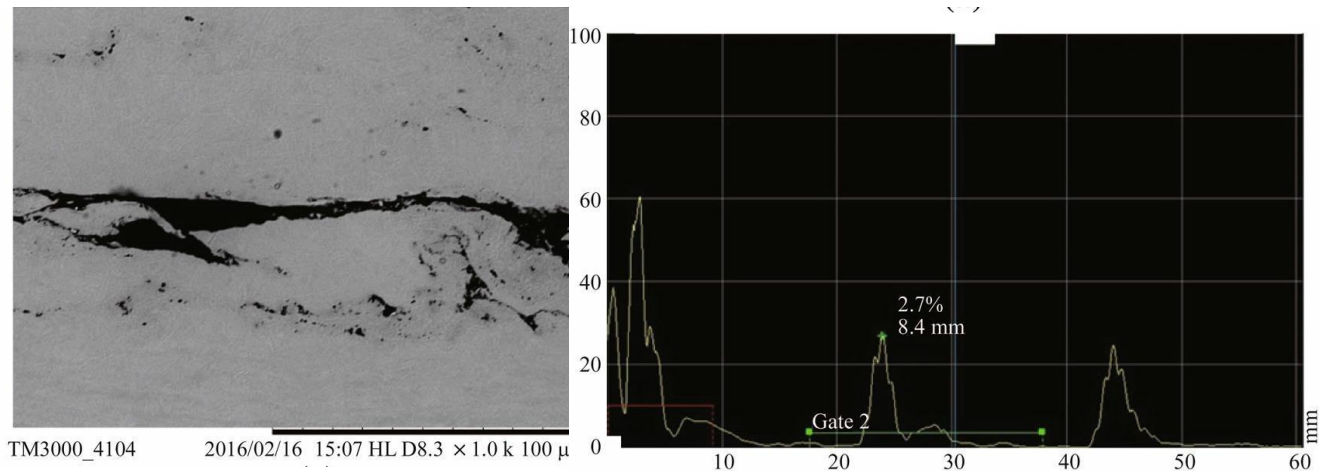


Fig. 14 – Macrograph of a joint with a big internal defect and the output of the respective ultrasonic control

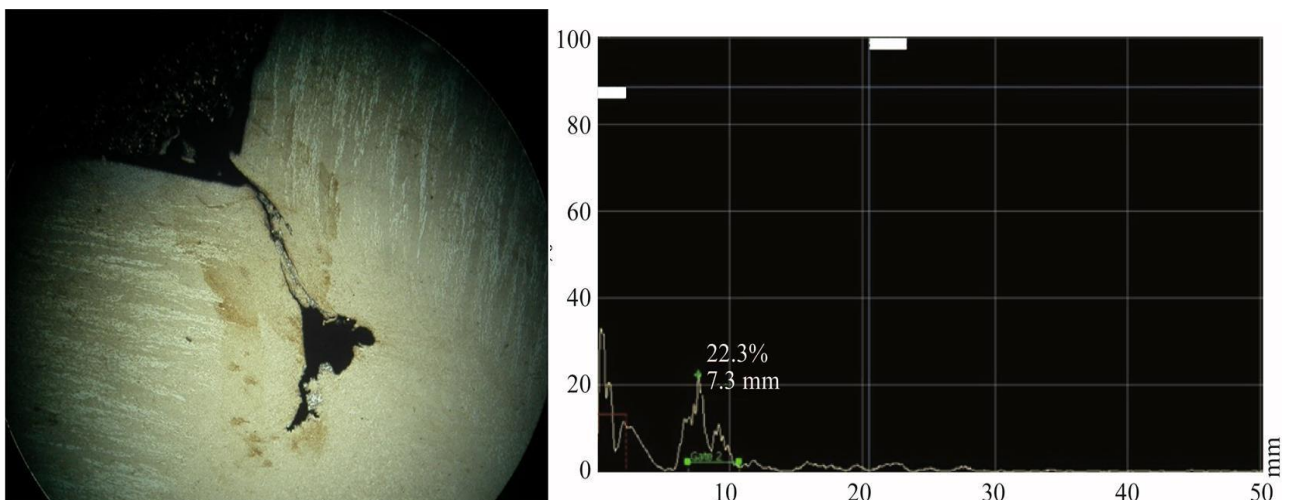


Fig. 15 - Macrograph of a joint with an internal defect and the output of the respective ultrasonic control

Figure 16 shows a macrograph of a joint with a kissing bond defect, highlighted by the black arrow, and the related output of the ultrasonic control. Once again the ultrasonic control is able to detect this typology of defect, and the respective output is different with respect to the ones regarding the other defects above described.

In figure 17 are reported two interesting diagrams that show, regarding the joints free from defects, the amplitude of the measured signal against, respectively, the extension of the welded zone (see Fig. 17a) and the extension of the thermo-mechanical affected zone TMAZ (see Fig. 17b). Looking at the above presented diagrams it is possible to observe that the amplitude of the signal increases with the increasing extension of the weld zone and decreases with the increasing extension of the TMAZ. It is important to remember that, as discussed in the previous section, the welded zone and the TMAZ have different microstructures. This suggests that the amplitude of the signal is influenced by the microstructure of the material, and the ultrasonic control, if properly analyzed, can give interesting information concerning the microstructure of the joint and the extension of the different metallurgical zones.

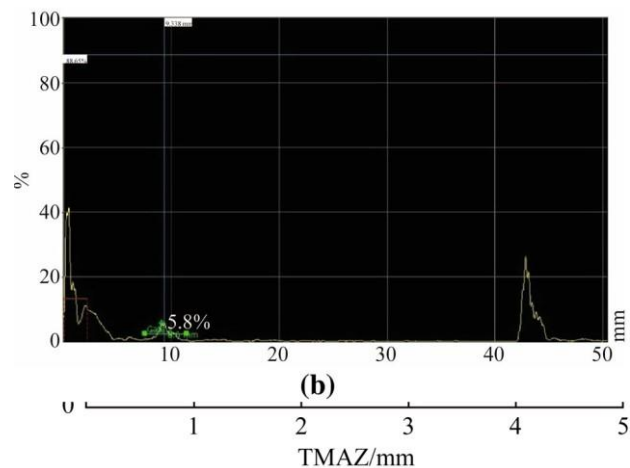


Fig. 16 – Macrograph of a joint with a kissing bond defect and the output of the respective ultrasonic control

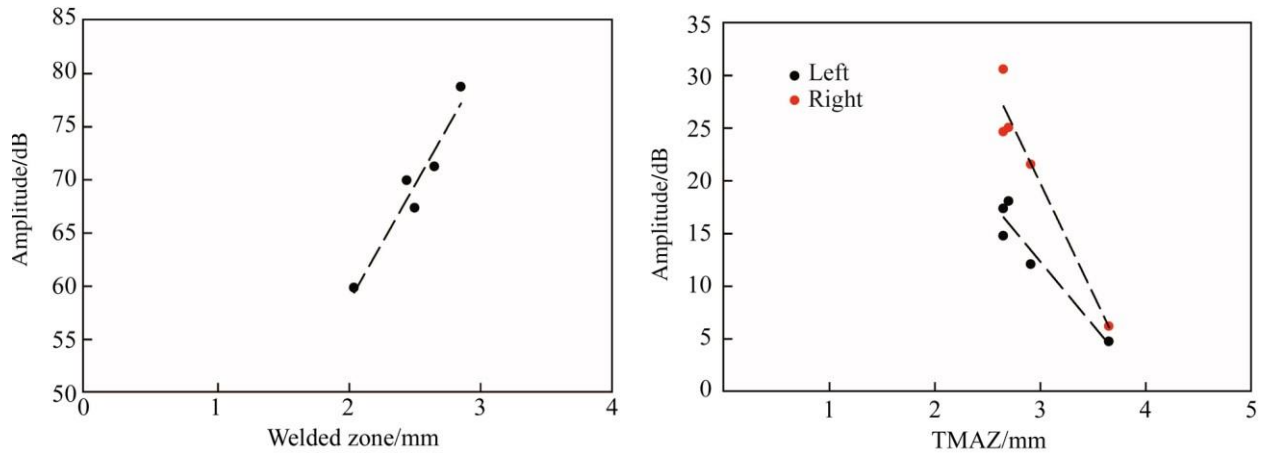


Fig.17 - Amplitude of the measured signal plotted against the extension of the welded zone and the extension of the thermomechanical affected zone TMAZ

3.1.3 Final observation on Traditional T-Joints

In order to resume the LFW parameters to be used in the experimental campaign dedicated to the EBM Joints, some interpolation plans and curves have been traced with the aid of Matlab- Curve Fitting Tool. In particular, the focus is on the extension of WZ and TMAZ and on the thickness of the α lamellae both in the WZ microstructure that in the TMAZ microstructure. With the aid of the interpolation curves, it can be possible to decide the couple of parameters (frequency and forging force) to use, to have the best results, in term of microstructure of the final LFW Joint. In fig. 18 and 19 are reported the results about the extension of the TMAZ and WZ zone and in fig.20 and 21 are reported the curves for what regards the thickness of the α lamellae in the WZ and in the TMAZ.

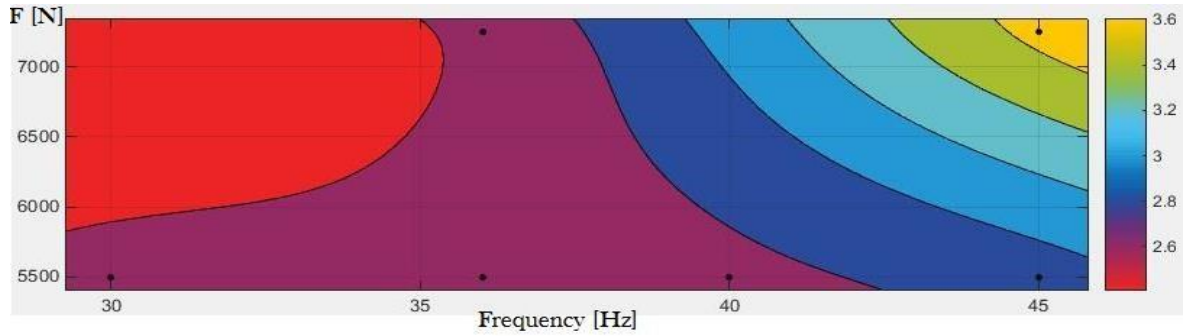


Fig.19- Interpolation curves of the extension of the TMAZ with respect to the frequency and the forging force. The column on the right reports the thickness in mm of the extension of the TMAZ.

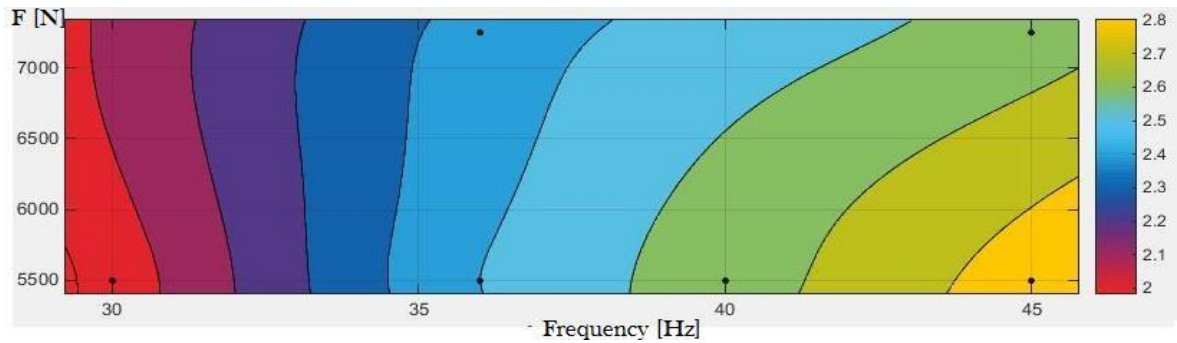


Fig.20- Interpolation curves of the extension of the WZ with respect to the frequency and the forging force. The column on the right reports the thickness in mm of the extension of the WZ.

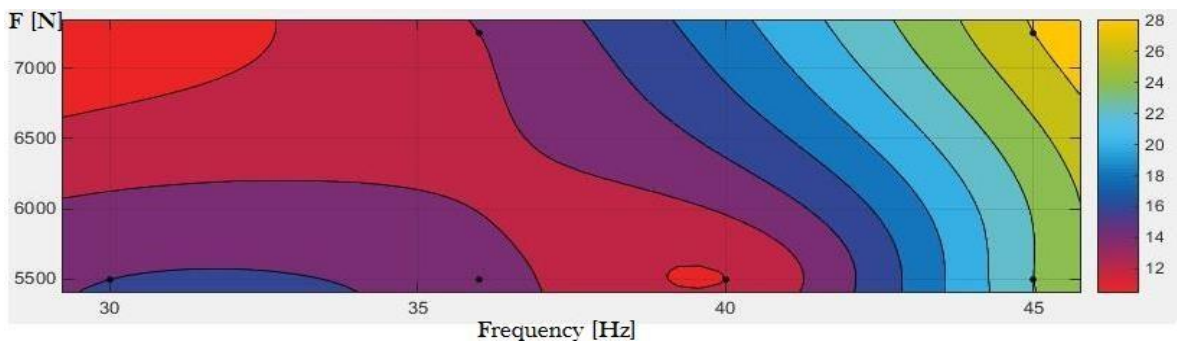


Fig.21- Interpolation curves of the thickness of the α lamellae in the TMAZ with respect to the frequency and the forging force. The column on the right reports the thickness in mm of the α lamellae in the TMAZ.

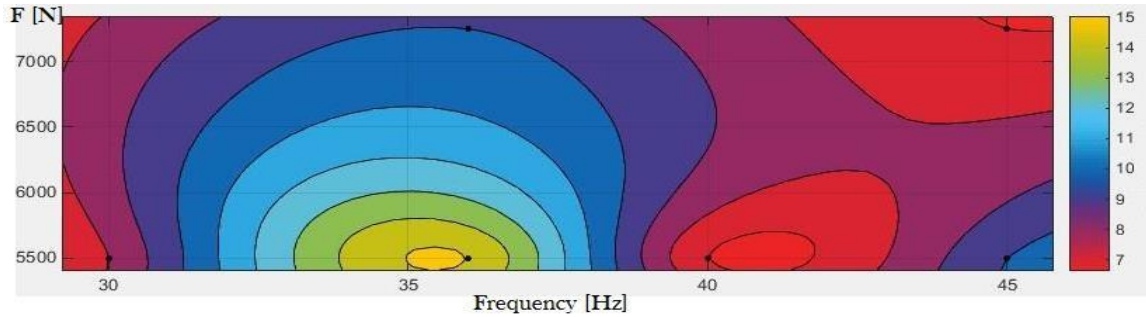


Fig.22- Interpolation curves of the thickness of the α lamellae in the WZ with respect to the frequency and the forging force. The column on the right reports the thickness in mm of the α lamellae in the WZ.

In order to obtain the bigger extension of both TMAZ and WZ (the zones with the best mechanical characteristics) it is coveted a frequency between 40 and 45Hz and the lowest forging force of 5500 N. In reality, it can be observed that also with a high forging force and the lowest frequency of 30Hz it is possible to obtain that result, but as discussed before with 30Hz the joints presents internal defects. For what regards the thickness of the α lamellae the best frequency to be used is the one of 40Hz and there is no strong correlation with the forging force. In conclusion, in order to combine both the beneficial effects of the extension of the interested zones and of the smallest thickness of the α grains, it will be used the frequency of 40Hz and the force of 5500N.

3.2- The EBM T-Joints

In Fig.23 the macrograph of the weld zone is reported. Parent Material, Thermo Mechanical Affected Zone and Weld Zone can be distinguished. The joint is sound without crack or other macroscopic defect.

More in details the Base Material (Fig. 24) is characterized by the presence of horizontal stratification and elongated structures in the direction of heat flux. The horizontal stratification corresponds to the different layers added during the EBM process. During the EBM process the cooling of melted Ti6Al4V generates in first β phase, further cooling produces the typical $\alpha+\beta$ structures. The elongated structures are the former beta grains mentioned above. They grew in

epitaxial way due to the presence of substantially unidirectional heat flow [35]. From β grains the α -lamellae originate, the lamellae are separated each other by β phase. Whole $\alpha+\beta$ structure is Widmanstätten type. From the boundary of the former β grains the alpha layer originates, it is a continuous string made entirely of α phase (Fig. 25) [35].

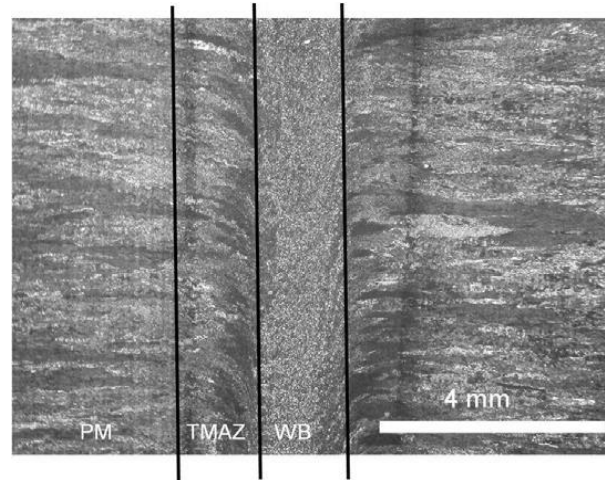


Fig.23 – Macrograph showing the different zones characteristic of the EBM T-Joint: Base Material, TMAZ and WZ.

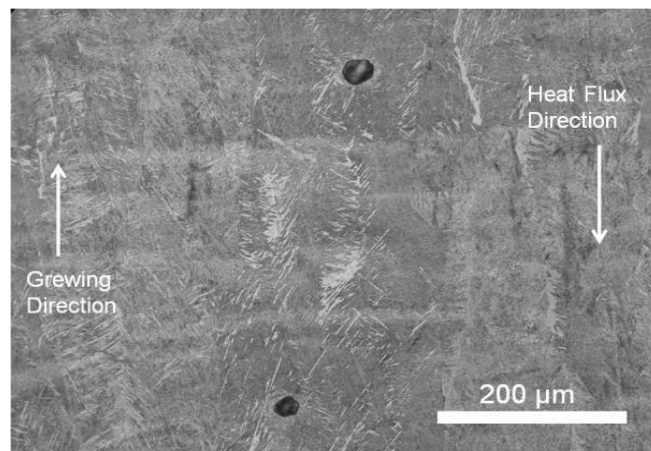


Fig.24- Macrograph of the Base Material in which can be noticed some porosities and the representation of the heat flux direction against the growing direction

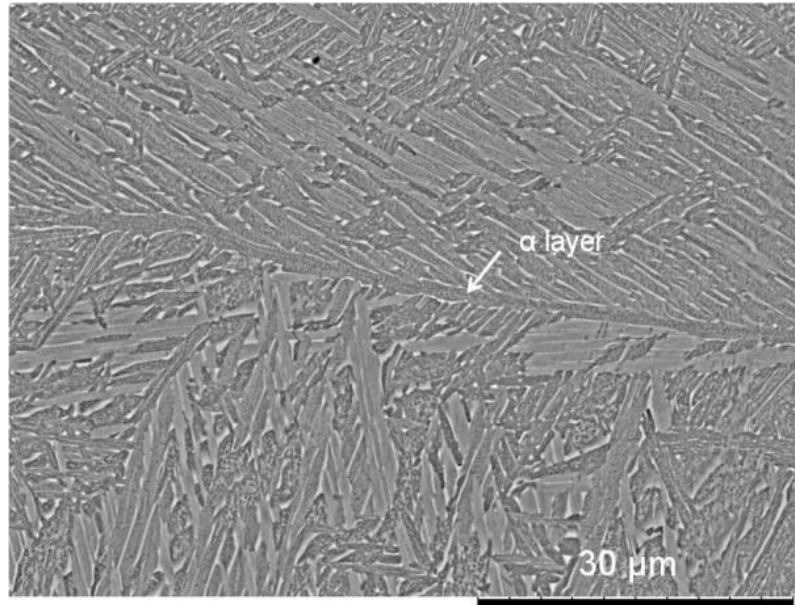


Fig. 25- Macrograph in which it is possible to notice the α layer from two layers of Ti6Al4V deposited material

Inside base material two different type of porosity can be distinguished. The first (Fig. 26) consists of round shaped pores of about 40 μm . The origin of these pores is attributed to the presence of gases that evolve during the melting process. In fact the Ti6Al4V lattice contains dissolved atoms of C, N, O that at melting point are released forming gas molecules. Another source of gases is the sublimation of the different component of the alloy. The second type of porosity (Fig. 27) consists of irregular shaped pores whose dimension is few microns. The presence of those pores is due to compaction defect inside the powder bed during the EBM process.

The microstructure of TMAZ is reported in Fig. 28, the former beta grains are still distinguishable, but they are deformed. In some areas of TMAZ a change in microstructure occurs. As showed in Fig. 29 a basket-wave microstructure is present. The presence of this type of structure is attributed to phenomena of recrystallization that occurs when the material experiences heating above the β -transus followed by a cooling faster to respect PM.

Again in TMAZ some small areas characterized, in comparison to PM, by both a change in composition and morphology of β phases can be noticed. In Fig. 30 the results of EDS analysis performed on aforementioned areas and on β phase of PM are reported. Those differences are attributed to local diffusion phenomena caused by the combined effect of deformation and heat.

In Fig. 31 the microstructure of WB is reported. It is martensitic type that means that the material experienced rapid cooling from temperature above the β -transus. Finally in both TMAZ and WB a considerable decrease of the porosity is observed.

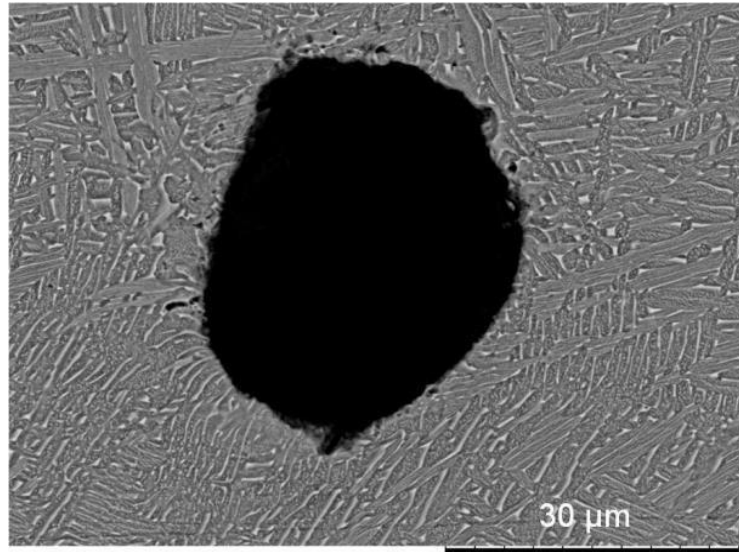


Fig.26- Micrograph of a Round Shaped Pore in the Base Material

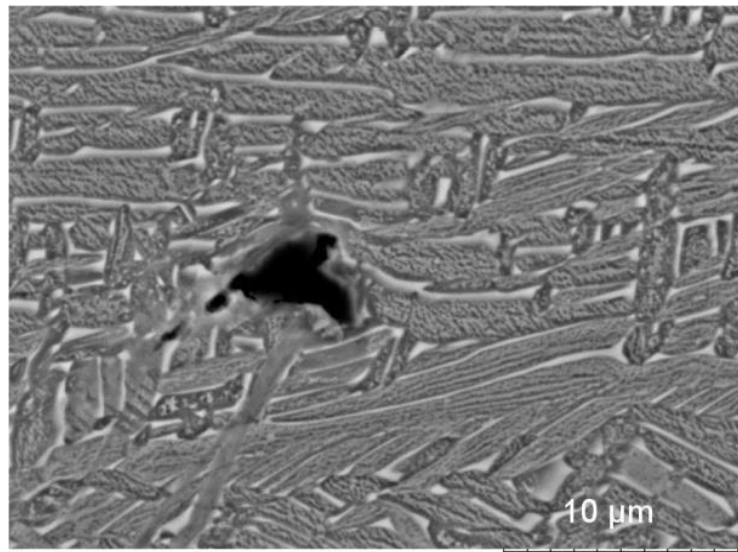


Fig.27- Micrograph of an Irregular Shaped Pore in the Base Material

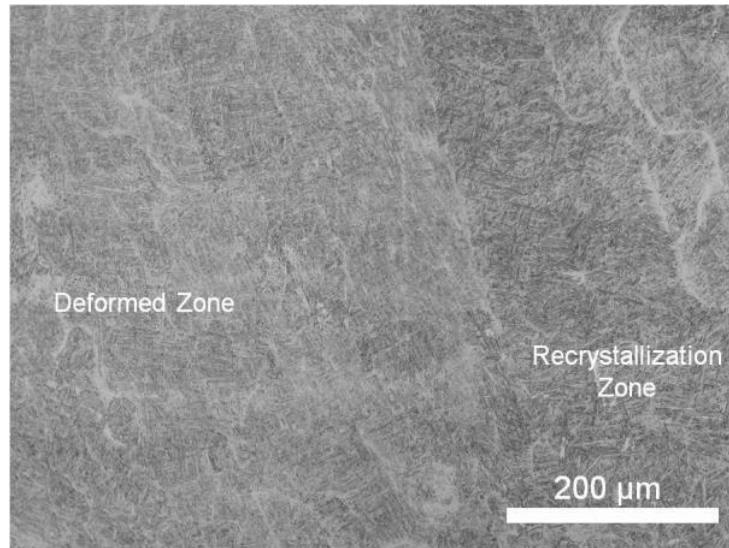


Fig.28- Macrograph of the TMAZ

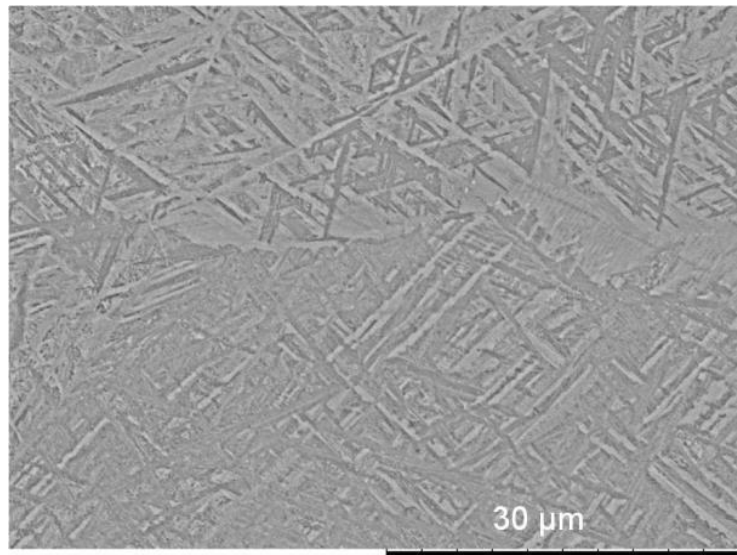


Fig.29- Micrograph of the TMAZ, a basket-wave structure can be noticed

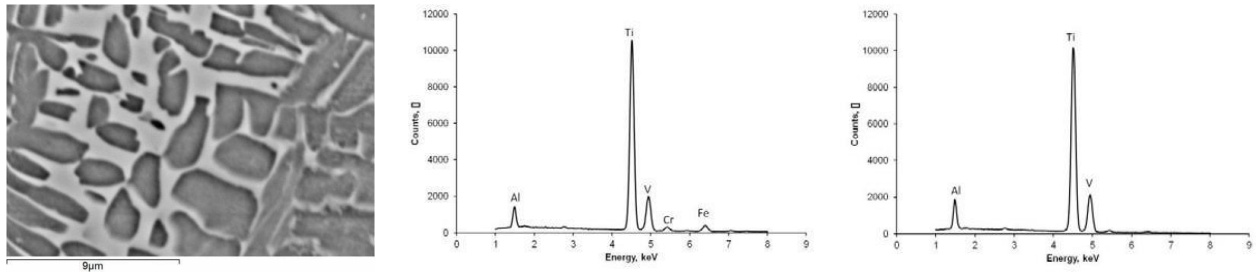


Fig.30 – EDS Results in the TMAZ in the α grains and in the β Phase

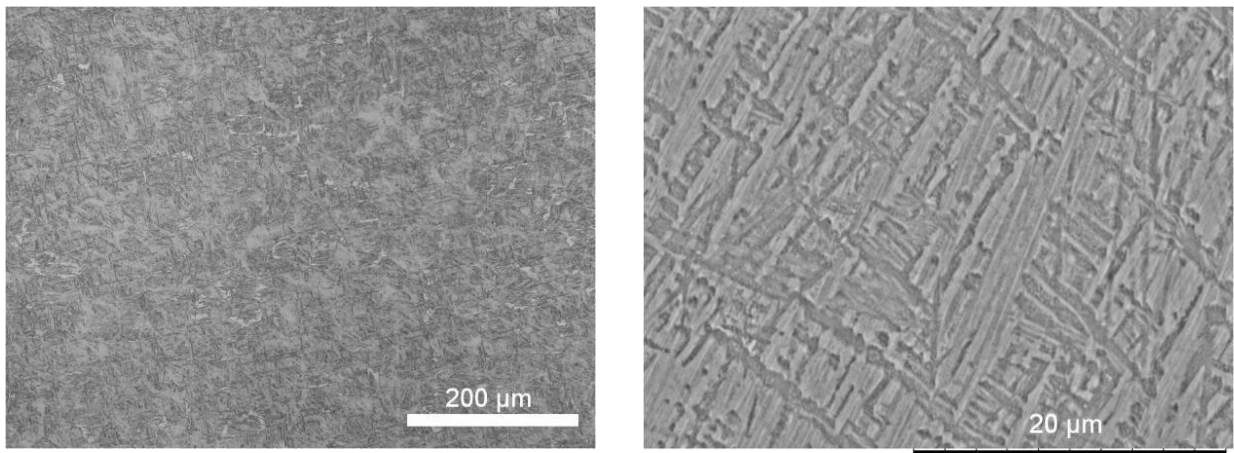


Fig.31- Macrograph and Micrograph of the WZ

3.2.1- Final observation on the EBM T-Joints

On the basis of the results discussed above the following conclusion can be deduced that due to the porosity in the Base Material used for the EMB Process, a focus on the Ti6Al4V powder will be done.

3.3- The Ti6Al4V Powder used in the EBM Process

The microstructure of the powder is shown in Fig. 32 in the previous section. It is possible to observe that the powder has a martensitic microstructure, characterized by very thin alpha needles, as a result of the high cooling rates during the gas atomization process. In Fig. 32 is

showed a particle free from defects, but some of the examined particles showed internal defects. In Fig.33, SEM micrographs of two particles with two different typologies of internal defects are shown.

In Fig. 33.a, a particle with a big round-shaped internal cavity is shown, which suggests that the cavity is filled with a gas under pressure. In Fig.33.b, conversely, a particle with some small internal porosities is shown. The irregular shape of these porosities suggests the absence of any internal gas. This latter defect is produced during the gas atomization process due to the fast solidification of the material in absence of any feed-head that feeds molten metal during the solidification to compensate the shrinkage phenomena that occur during the phase transition and in the successive cooling.

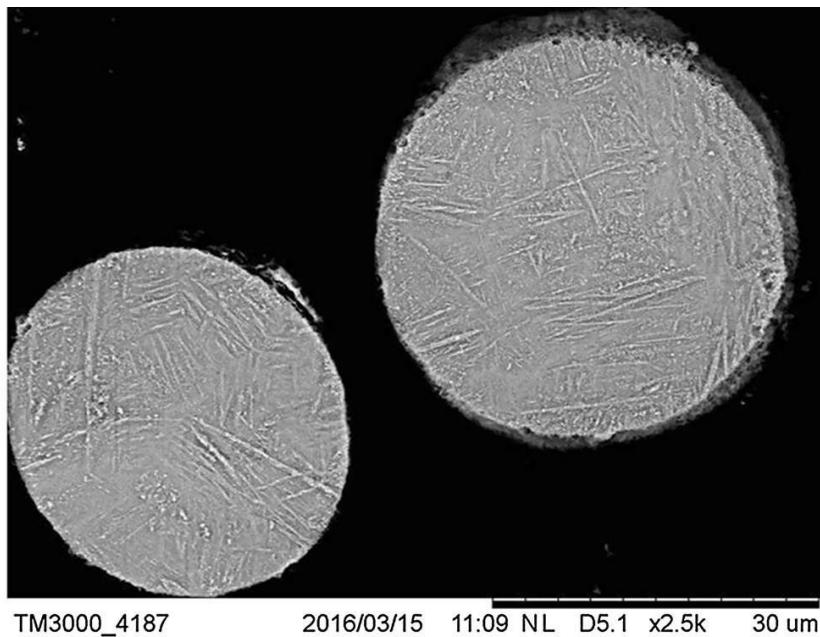


Fig. 32 – Round Shaped Powder of Ti6Al4V used for the EBM process to get the ingots for the EBM T-Joints.

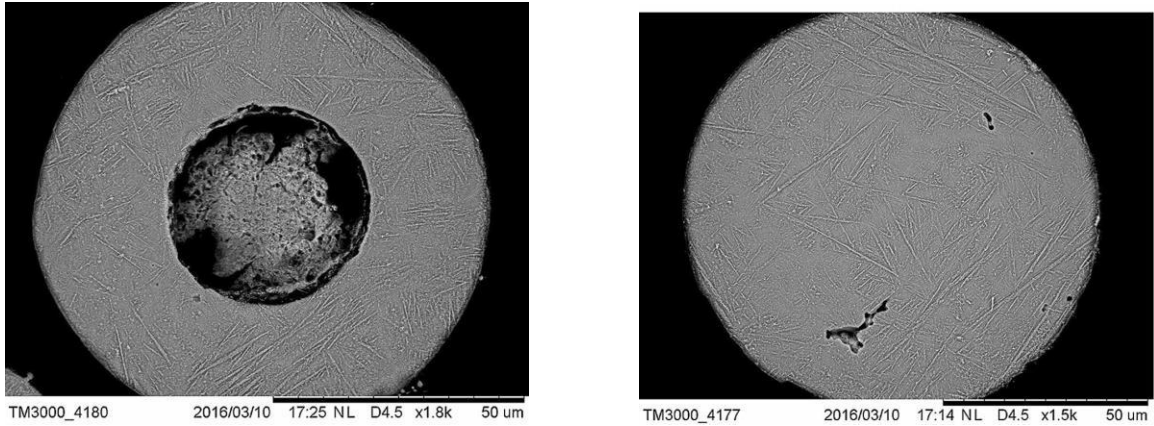


Fig. 33- 33.a Internal Round Shaped Defect, 33.b Internal Irregular Shaped Defect

Defects were observed in all the analyzed EBM ingots.

These defects are different in shape and have a different origin, so they can be classified in different categories.

In Fig. 34, a particle of powder that was not completely melted during the building process can be observed, this is a typical defect of the process and is due to an ineffective heat transfer within the powder bed.

The position of the defects within the additive manufactured ingots was studied. In Fig. 35, a low-magnification image of the cross section in which are visible different defects is shown. In particular are appreciable voids with different shape and in different positions. Some voids are located among two consecutive laser tracks and some others are located within a single laser track. In Fig. 36 is highlighted a big porosity located at the boundary among different particles. As will be further discussed, the different position and the different shape suggest a different formation mechanism for the defects.

In Fig. 37, voids with an elongated shape are shown. These voids could be keyholes, as shown in the defects discussed in literature [36, 37], and were induced during the additive manufacturing process. The lower surfaces of the voids are relatively flat, and this suggests that this is the top surface of the layer beneath the void. Observations of void locations and morphology suggest that voids were formed due to localized ineffective melting.

In Fig. 38, different voids can be observed. These voids have an irregular shape, this suggest that there are no gases within this pores. As documented in literature [38] the formation of these

pores is due to an ineffective heat transfer in the powder bed, these pores can be found in the middle of a particular stratification layer.

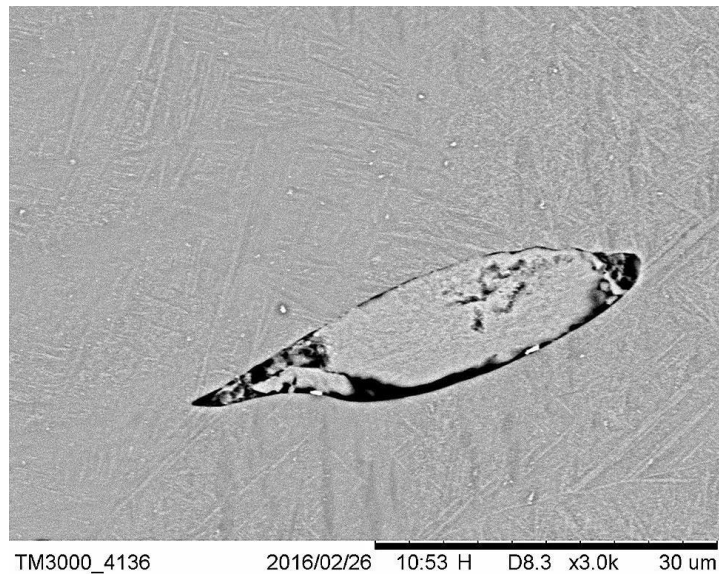


Fig. 34- Cross section of the EBM ingot, an unmelted particle of powder embedded within the component is visible

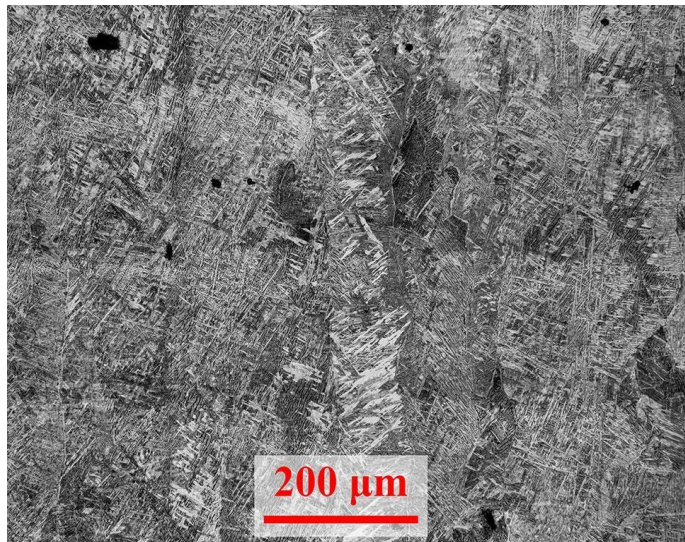


Fig. 35- Low-magnification cross section micrograph in which some voids and the stratification effect are appreciable

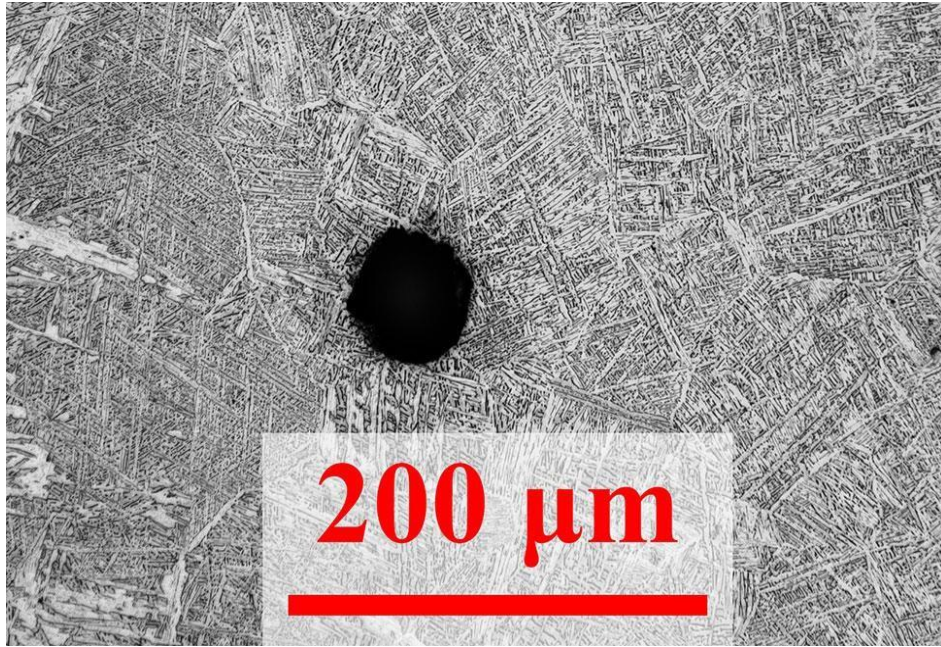


Fig. 36 - Porosity located at the boundary among different particles

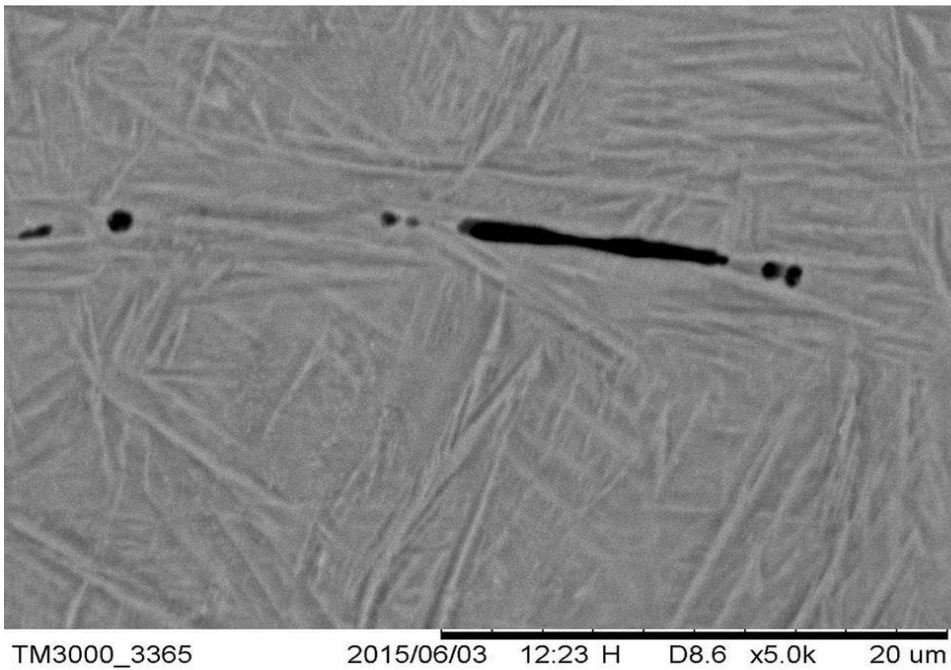


Fig. 37- Keyhole defect, it can be noticed the elongated shape

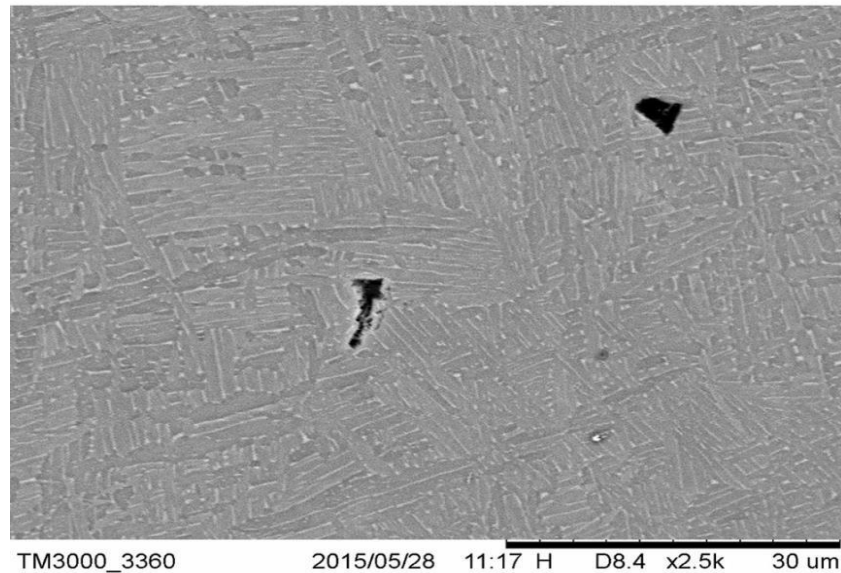


Fig. 38 – Irregular Shaped Pores within the Ingot

In Fig. 39, micrographs in which voids with a spherical shape but with different dimensions can be observed are shown. The presence of these voids can be addressed to the porosity detected within the powders. In particular, the spherical shape of the voids observed in Fig. 39 suggests the presence of gas entrapped within the void itself. The voids of bigger dimension, Fig. 39.a, are due to gas inclusion during the building process; conversely, the voids of small dimensions, Fig. 39.b, are due to porosity of the starting powders, in fact the dimension of these voids is comparable with the porosities observed within the starting powders.

By using an image analysis software, the size distribution of the voids was measured and is reported in Fig. 40, where n/nt is the number of the voids in a particular size range versus the total number of observed voids, i.e., is the fraction of voids with a given size.

It is evident that the most of the defects are in the size range between 0 and 10 microns. Indeed, this is the size range of the defects that were observed within the starting powders.

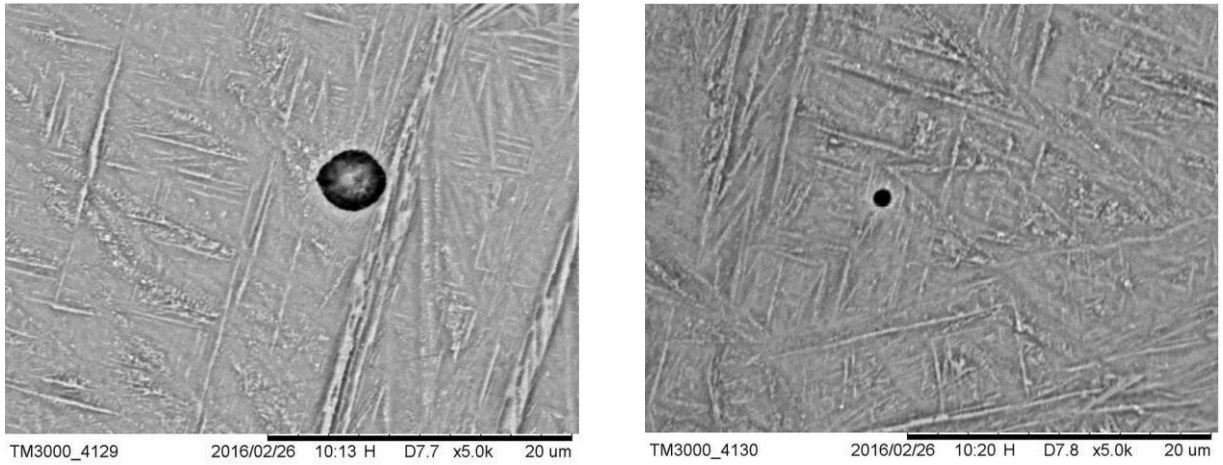


Fig. 39 – Round Shaped Defects with two different dimensions

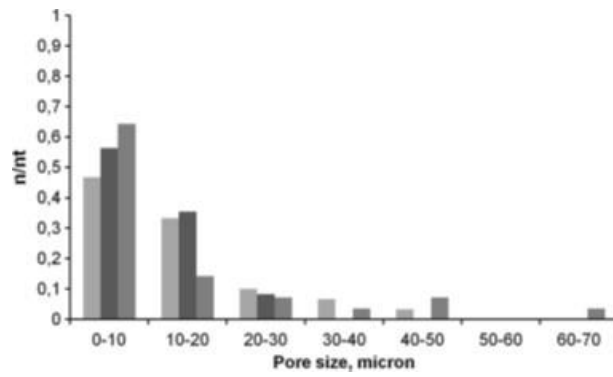


Fig.40 - Measured size distribution of the voids in the three direction of observation

4- Conclusions and Future Development

In conclusion in the first part of the experimental campaign of the Traditional T-Joints has been observed that:

- The different set of process parameters adopted allowed obtaining joints with different properties. The joints free from defects and joints with different typologies of defects, i.e., internal porosities, internal big defects and kissing bonds, were produced.
- The metallurgy of the joints was the one typically produced by the LFW process. It is possible to observe a TMAZ made of deformed grains within an $\alpha+\beta$ matrix and a welded zone made of fully-recrystallized grains in which it is possible to observe a Widmanstatten microstructure produced by the fast cooling from the b region.
- The joints free from defects were manufactured joints with different grain sizes and different extensions of the metallurgical zones produced by the welding, i.e., the WZ and the TMAZ.
- The results of the ultrasonic control proved the effectiveness of this method in detecting the internal defects of LFW titanium joints. It was possible to detect and distinguish different typology of defects.
- The measured amplitude of the signal is influenced by the microstructure of the joint, which will allow having information regarding the microstructure through the ultrasonic control.
- The optimum parameters set in terms of frequency and forging force, in order to have an extended TMAZ and WZ and thin alpha lamellae, respectively are of 40Hz and 5500N.

In the study of the EBM T-Joints has been find out that:

- The LFW process applied to EBMed Ti6Al4V specimens produces sound joints.

- Both in WZ and TMAZ a decrease in porosity is observed with respect to the Base Material.
- In the TMAZ recrystallization and redistribution of alloy components occurs.
- The WZ has a martensitic microstructure that indicates fast cooling from temperature above the β -transus.
- The internal defects found in the Base Material indicates that the Ti6Al4V powder used for the EBM process to get the ingots for the joints are affected by initial porosities.

The focus done on the Ti6Al4V powder shows that:

- All the components manufactured showed internal defects.
- Different typologies of defect were presented and discussed. Some spherical voids detected within the ingots are directly related to the pores observed within the powder.
- The spherical shaped pores are full of internal gas coming from the gas atomizing process to get the Ti6Al4V powder. This kind of defect can generate the starting point of a crack.
- The Keyhole and Irregular shaped pores are free from internal gas.
- In order to obtain printed components free from defects, particularly attention must be paid to the starting powder. In particular, it is mandatory to carefully control the gas atomization process, or to change the type of powder used, in order to obtain powder free from porosities and above all powder without gas. In fact, the porosities within the powder could be reduced during the printing process but the entrapped gas remains within the component resulting in the observed spherical-shaped voids.

Bibliography

- 1- E. Herderick, *Additive Manufacturing of Metals: A Review, Proceedings of MS&T_11, Additive Manufacturing of Metals, Columbus, OH, 2011*
- 2- NIST, “*Measurement Science Roadmap for Metal-Based Additive Manufacturing,*” US Department of Commerce, National Institute of Standards and Technology, Prepared by Energetics Incorporated, May 2013
- 3- J. Scott, N. Gupta, C. Weber, S. Newsome, T. Wohlers, and T. Caffrey, *Additive Manufacturing: Status and Opportunities, IDA, Science and Technology Policy Institute, Washington, DC, 2012*
- 4- DoD SBIR/STTR Database (<https://www.dodsbir.net>), Contracts N00014-12-C-0411, N00014-12-C-0221, N00014-13-C-0057, Nov 2013
- 5- S.M. Kelly and S.L. Kampe, *Microstructural Evolution in Laser- Deposited Multilayer Ti-6Al-4V Builds: Part II. Thermal Modeling, Metall. Trans. A., 2004, 35A, p 1869–1879*
- 6- F. Wang, S. Williams, P. Colegrove, and A.A. Antonysamy, *Microstructure and Mechanical Properties of Wire and Arc Additive Manufactured Ti-6Al-4V, Metall. Trans. A., 2013, 44A, p 968–977*
- 7- B. Zheng, Y. Zhou, J.E. Smugeresky, J.M. Schoenung, and E.J. Lavernia, *Thermal Behavior and Microstructural Evolution during Laser Deposition with Laser-Engineered Net Shaping: Part I. Numerical Calculations, Metall. Trans. A., 2013, 39A, p 2237–2245*
- 8- T. Vilaro, C. Colin, and J.D. Bartout, *As-fabricated and Heat-Treated Microstructures of the Ti-6Al-4V Alloy Processed by Selective Laser Melting, Metall. Trans. A., 2011, 42A, p 3190–3199*

- 9- B. Zheng, Y. Zhou, J.E. Smugeresky, J.M. Schoenung, and E.J. Lavernia, *Thermal Behavior and Microstructure Evolution during Laser Deposition with Laser-Engineered Net Shaping: Part II. Experimental Investigation and Discussion*, *Metall. Trans. A.*, 2008, 39A, p 2228
- 10- P.A. Kobryn and S.L. Semiatin, *The Laser Additive Manufacturing of Ti-6Al-4V*, *JOM*, 2011, 53, p 40–43
- 11- L.E. Murr, E. Martinez, S.M. Gaytan, D.A. Ramirez, B.I. Machado, P.W. Shindo, J.L. Martinez, F. Medina, J. Wooten, D. Ciscel, U. Ackelid, and R.B. Wicker, *Microstructural Architecture, Microstructures, and Mechanical Properties of a Nickel-Base Superalloy Fabricated by Electron Beam Melting*, *Metall. Trans. A.*, 2011, 42A, p 3491– 3508
- 12- S.G. Lambrakos and K.P. Cooper, *An Algorithm for Inverse Modeling of Layer-by-Layer Deposition Processes*, *JMEP*, 2009, 18(3), p 221– 230
- 13- S.G. Lambrakos and K.P. Cooper, *A General Algorithm for Inverse Modeling of Layer-by-Layer Deposition Processes*, *JMEP*, 2010, 19(3), p 314–324
- 14- F. Wang, S. Williams, P. Colegrove, and A.A. Antonysamy, *Microstructure and Mechanical Properties of Wire and Arc Additive Manufactured Ti-6Al-4V*, *Metall. Trans. A.*, 2013, 44A, p 968–977
- 15- AMS 4999 Specification, *Titanium Alloy Laser Deposited Products 6Al-4V Annealed*, SAE, Warrendale, PA 2002
- 16- S. Rengers, *Electron Beam Melting [EBM] vs. Direct Metal Laser Sintering [DMLS]*, Presented at SAMPE Midwest Chapter, Direct Part Manufacturing Workshop, Wright State University, Nov 2012

- 17- M. Svensson, *Ti6Al4V manufactured with Electron Beam Melting (EBM): Mechanical and Chemical Properties, Presented at Aeromat 2009, Dayton OH, Jun 2009*
- 18- M.K.E. Ramosoou, G. Booysen, T.N. Ngonda, and H.K. Chikwanda, *Mechanical Properties of Direct Laser Sintered Ti-6Al-V4, MS&T_11, Columbus, OH, 2011*
- 19- 1. Zhao P, Fu L, Chen H (2016) *Low cycle fatigue properties of linear friction welded joint of TC11 and TC17 titanium alloys. J Alloy Compd 675:248–256*
- 20- Wang SQ, Ma TJ, Li WY et al (2016) *Microstructure and fatigue properties of linear friction welded TC4 titanium alloy joints. Sci Technol Weld Join 2:1–5*
- 21- Astarita A, Scherillo F, Curioni M et al (2016) *Study of the linear friction welding process of dissimilar Ti-6Al-4V—stainless steel joints. Mater Manuf Process. doi:10.1080/10426914.2016.1151048*
- 22- Ji Y, Zhang T, Guo D et al (2016) *Structure and mechanical property of DD6/FGH96 linear friction welding joint. Hanjie Xuebao/Trans China Weld Inst 37(4):111–114*
- 23- Chen X, Xie FQ, Ma TJ et al (2016) *Effects of post-weld heat treatment on microstructure and mechanical properties of linear friction welded Ti2AlNb alloy. Mater Des 94:45–53*
- 24- Vairis A (2010) *Linear and rotary friction welding review. Int Mater Rev. doi:10.1080/09507110903569149*
- 25- Ma TJ, Chen X, Li WY et al (2016) *Microstructure and mechanical property of linear friction welded nickel-based superalloy joint. Mater Des 89:85–93*
- 26- Zhang CC, Zhang TC, Ji YJ et al (2015) *Formation process and mechanism of linear friction welding joint. J Mater Eng 43(11):39 43*

- 27- Vairis A, Frost M (1998) *High frequency linear friction welding of a titanium alloy. Wear* 217(1):117–131
- 28- Rao HM, Ghaffari B, Yuan W et al (2016) *Effect of process parameters on microstructure and mechanical behaviors of friction stir linear welded aluminum to magnesium. Mater Sci Eng A* 651:27–36
- 29- Buffa G, Cammalleri M, Campanella D et al (2015) *Linear friction welding of dissimilar AA6082 and AA2011 aluminum alloys: microstructural characterization and design guidelines. Int J Mater Form* 22:1–9
- 30- Impero F, Scherillo F, Astarita A et al (2015) *Study of the metallurgy of dissimilar Ti-6Al-4V-stainless steel linear friction welded joints. Key Eng Mater* 651–653:1427–1432
- 31- Bhamji I, Preuss M, Threadgill PL et al (2010) *Linear friction welding of AISI 316L stainless steel. Mater Sci Eng A* 528:680. doi:10.1016/j.msea.2010.09.043
- 32- Karadge M, Preuss M, Lovell C et al (2007) *Texture development in Ti-6Al-4V linear friction welds. Mater Sci Eng A* 459:182–191
- 33- Ma TJ, Chen T, Wen Y et al (2011) *Formation mechanism of linear friction welded Ti-6Al-4V alloy joint based on microstructure observation. Mater Charact* 62:130–135
- 34- Li B, Shen Y, Hu W (2011) *The study on defects in aluminum 2219-T6 thick butt friction stir welds with the application of multiple non-destructive testing methods. Mater Des* 32:2073–2084
- 35- G. Lutjering, J.C. Williams: *Titanium*, Springer, Berlin, 2003
- 36- H. Attar, M. Calin, L.C. Zhang, S. Scudino, and J. Eckert, *Manufacture by Selective Laser Melting and Mechanical Behavior of Commercially Pure Titanium, Mater. Sci. Eng., A*, 2014, 593, p 170–177

37- N. Hrabe, T. Gnäupel-Herold, and T. Quinn, *Fatigue Properties of a Titanium Alloy (Ti-6Al-4V) Fabricated Via Electron Beam Melting (EBM): Effects of Internal Defects and Residual Stress*, *Int. J. Fatigue*, 2016, doi:10.1016/j.ijfatigue.2016.04.022

38- Y. Zhai, H. Galarraga, and D.A. Lados, *Microstructure Evolution, Tensile Properties, and Fatigue Damage Mechanisms in Ti-6Al-4V Alloys Fabricated by Two Additive Manufacturing Techniques*, *Proc. Eng.*, 2015, 114, p 658–666